RTSense: Passive RFID based Temperature Sensing

Swadhin Pradhan
UT Austin, USA

Lili Qiu
UT Austin, USA

ABSTRACT

Passive radio-frequency identification (RFID) tags are attractive because they are low cost, battery-free, and easy to deploy. This technology is traditionally being used to identify tags attached to the objects. In this paper, we explore the feasibility of turning passive RFID tags into battery-free temperature sensors. The impedance of the RFID tag changes with the temperature and this change will be manifested in the reflected signal from the tag. This opens up an opportunity to realize battery-free temperature sensing using a passive RFID tag with already deployed Commercial Off-the-Shelf (COTS) RFID reader-antenna infrastructure in supply chain management or inventory tracking. However, it is challenging to achieve high accuracy and robustness against the changes in the environment. To address these challenges, we first develop a detailed analytical model to capture the impact of temperature change on the tag impedance and the resulting phase of the reflected signal. We then build a system that uses a pair of tags, which respond differently to the temperature change to cancel out other environmental impacts. Using extensive evaluation, we show our model is accurate and our system can estimate the temperature within a 2.9 degree centigrade median error and support a normal read range of 3.5 m in an environment-independent manner.

CCS CONCEPTS

• **Computer systems organization → Sensor networks**.

KEYWORDS

impedance, passive rfid, temperature sensing, smart spaces

Swadhin Pradhan and Lili Qiu. 2020. RTSense: Passive RFID based Temperature Sensing. In *The 18th ACM Conference on Embedded Networked Sensor Systems (SenSys '20), November 16–19, 2020, Virtual Event, Japan.* ACM, New York, NY, USA, 14 pages. https://doi.org/10.1145/3384419.3430729

1 INTRODUCTION

Motivation: Accurate temperature sensing is desirable in many environments, such as warehouse, greenhouse, and buildings. These places require maintaining 55° and 80° Fahrenheit (F) (12-27 ° centigrade) [1]. Fine-grained temperature sensing can save up to 45% of the building energy consumption [2] while promoting the occupants' well-being [3–5], as people spend around 90% percent of their time indoors [6]. Furthermore, temperature monitoring is important to supply chain management, inventory maintenance, greenhouses, and health sectors. For example, greenhouses require monitoring temperature within a resolution of around 4° [7]. Temperature monitoring is also important for people's health, materials' life-time in health sectors [8], *heating, ventilation, and air conditioning* (HVAC) systems in hospitals and warehouses.

There is a significant variation in temperature across a building [9]. We also confirm this using empirical evaluation by measuring the temperature at a few locations on the same floor as shown in Fig. 1. Fig. 2 shows the temperature varies from 4° to 9° centigrade.

Figure 1: Building floor map and different temperature measurement sites. The box symbols and cross symbols denote floor-level and room-level locations, respectively.

Existing works: A natural approach is to deploy temperature sensors. However, temperature sensors not only are costly but also require batteries. Battery replacement is time-consuming and labor intensive [10]. For example, a commercial-off-the-shelf temperature sensor like [11] requires around 100mW power, which means continuous temperature sensing can only last for 10 hours using a coin-cell battery. Therefore, we seek to develop a battery-free temperature sensor, which can also be easily deployed. Passive RFID tags are battery-free and there has been already a wide-spread deployment of RFID infrastructure in supply chain management and inventory maintenance systems. Several works [12–15] propose adding micro-controllers to RFID tags to obtain and communicate

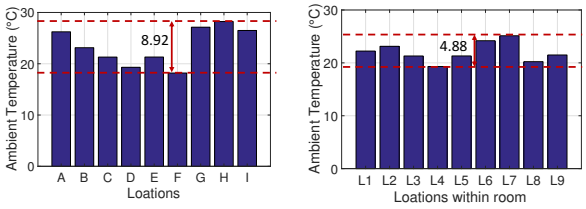

(a) Location Variation. (b) Room Variation.

Figure 2: Temperature varies across different locations and within the room. The temperature variation can go up to 9° centigrade (C). The ambient temperature snapshots are taken at 9 a.m. and 9 p.m. Non-uniform indoor temperature means ubiquitous temperature sensing is important for achieving indoor thermal comfort.

SenSys '20, November 16–19, 2020, Virtual Event, Japan

ACM ISBN 978-1-4503-7590-0/20/11…$15.00
https://doi.org/10.1145/3384419.3430729

the temperature information. However, micro-controllers significantly increase the cost of RFID tags, which limits its applicability.

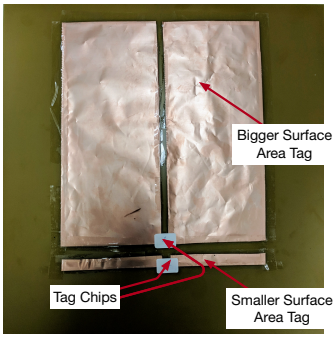

Figure 3: Tag-pair of RTSense.

Our approach: Inspired by the growing popularity of low-cost passive RFID tags, we explore the feasibility of turning passive RFID tags into battery-free temperature sensors. RFID is especially appealing since many large warehouses and greenhouses already deploy passive RFID tags for inventory tracking. If we can add temperature sensing capability to the already deployed tags, we do not incur additional hardware or deployment cost.

There have been several existing works that use RFID tags to sense motion, such as tracking [16, 17], activity monitoring [18, 19], or touch sensing [20]. However, temperature sensing is significantly different since it is beyond measuring the propagation path length but measuring the physical property of the antenna.

[15] reports that temperature change can result in a change in the impedance of the RFID tag and such a change can be captured by the phase of the signal reflected from the RFID tag. We experimentally confirm the observation [15]. Based on this relation, one can potentially map the phase change back to the temperature change. While intuitive, making it work well in practice involves several challenges: (i) how to achieve high accuracy, (ii) how to achieve robustness against other environmental change, and (iii) how to maintain a good sensing range [21].

Despite significant existing works on tag-antenna based sensing [15, 22, 23], the above challenges remain open. However, passive tag-antenna based approaches are promising for large scale deployment. In particular, [24] is closest to our work in this area of battery-free temperature sensing using passive RFID tags. It takes into account the environmental impact on the design and uses a Commercial Off-the-Shelf (COTS) setup. However, its sensing resolution is coarse since it uses power-based metric [21, 25]. The commercial reader can only adjust the power at coarse granularity (*e.g.*, 0.3 dBm [26]), which limits the sensing accuracy. Its communication range is 2m, much lower than the typical RFID range of 6m, since it adds an external sensor to the tag antenna and causes a large impedance mismatch with the chip, which reduces the range.

To address (i), we develop an analytical model that captures the impact of temperature change on the phase of the reflected signal. Based on the model, we observe that a larger antenna has a larger impedance change for the same amount of temperature change. Therefore, we increase the antenna size to improve resolution. We further use larger bandwidth and multiple well-separated antennas to improve sensing accuracy.

To address (ii), we use a pair of tags with different sizes, which respond differently to the temperature change. We measure the phase difference between the two tags. The use of two tags allows us to cancel out the impact of other environmental changes. We build the tag-pair by attaching RFID chip transponders to the dipole antennas as shown in Fig. 3.

To achieve (iii), we select an appropriate antenna size to match with the chip impedance and maintain a normal range of 3-4 m. To the best of our knowledge, this is the *first* work that uses COTS passive RFID to measure temperature without any additional hardware (*e.g.*, temperature sensors). By using a tag-pair, it can work for different environments.

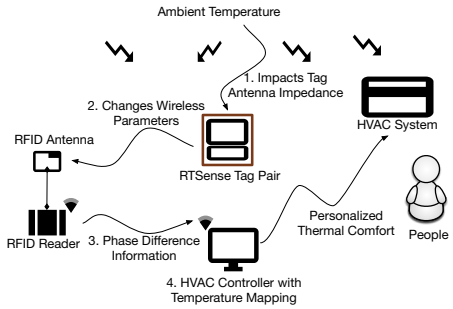

Figure 4: Design of RTSense.

Before arriving at the final design, we experiment with a variety of RFID setups for temperature sensing. Through experiments, we converge to a simple commercial RFID tag coupled with a custom-designed copper dipole antenna based temperature sensor. We build a system called RTSense (*R*FID-based *T*emperature Sensing), which can be easily deployed. It can be used to construct a room-level thermal map. We also use a metric based on the received phase to increase its robustness against other environmental changes. Fig. 4 shows the outline of RTSense. In this paper, we focus on the effectiveness of passive RFID based temperature sensing and leave the integration with HVAC to the future work.

To summarize, we make the following main contributions:

- We develop a simple yet accurate model that captures the relationship between the temperature and phase of the reflected signal from an RFID tag.
- We design a system of RFID tag-pair with different sizes as temperature sensors robust against environmental changes.
- We extensively evaluate our system and show that cheap passive RFID tags can serve as temperature sensors. It supports a normal read range (over 3m) with a median sensing error of 2.9° C.

Outline: The rest of the paper is organized as follows. First, We review related works in Sec. 2. We introduce RFID in Sec. 3. Next, we describe the analytical model behind RTSense in Sec. 4. Then we describe our system design in Sec. 5. We present our experimental setup in Sec. 6 and implementation in Sec. 7. We present our evaluation in Sec. 8. Finally, we conclude in Sec. 9.

2 RELATED WORK

We classify the related work into the following three classes: (i) active tag sensing, (ii) passive tag motion sensing, and (ii) sensing physical properties using passive RFID tags.

2.1 Active RFID-based Sensing

[27, 28] use active RFID tags with batteries as input. In this active tag based setup, the sensed value is stored on the tag chip memory, which will be forwarded to a reader. Examples include RFM3200, a wireless flexible temperature sensor WISPs [29] and Ekhonet [30]. The requirement of writing to the tag memory makes the tag costly. In contrast, RTSense uses inexpensive passive RFID tags that cost about 0.03 - 0.05 $ each.

2.2 Passive Tag Motion Sensing

RF-IDraw [16] develops a system to track motion using RFID with 8 cm median error with an antenna array. Moreover, *PolarDraw* [17] uses two linearly polarized COTS antennas and exploits polarization property to track a RFID tag. RFind [31] exploits larger bandwidth to enable fine-grained offline tracking of RFID tag. *Tagyro* [32] exploits phase information of multiple tags to get the orientation of the object. [33] uses a chip-less tag with a WiFi based customized setup to detect human object interaction. However, unlike RTSense, these works do not sense physical property of the environment, such as temperature.

System	Range	Resolution	Cost
Farsens EPC C1G2 Battery-less Ambient Temperature Sensor [34]	5 m (in Passive mode) and 20 m (in Battery-assisted mode)	1 degree	50 $ per tag & 1200 $ for reader/antenna [35].
RFID hacking [24]	2 m	20 degree	Few dollars for tag sensor & 1200$ for reader/antenna.
Embedded Sensor System-on-Chip Solution [36]	4 m	1 degree	Proposed design and not commercially available.
2510-TMP Temperature Sensing Tag [37]	5 m	10 degree	90$ per tag & 1400$ for custom reader/antenna.
RFM3200 Wireless Flexible Temperature Sensor [38]	5 m	Not specified	40$ per tag & 1400$ for custom reader/antenna.
Paraffin wax tag based Sensing [39]	2 m	20 degree	Proposed design for tag & 1400$ for custom reader/antenna.
Epidermal patch temperature Sensor [40]	1 m	10 degree	Proposed design for tag & 1200$ for reader/antenna.

Table 1: Summary of RFID Temperature Sensing Systems.

2.3 Passive Tags for Physical Sensing

Marocco et al. [41, 42] report that the tag RSS and phase change with the environment. This observation opens up the possibility of antenna-based environmental sensing. These mechanisms can support tags with and without chips in a COTS or customized setup [31]. [24] proposes adding a sensor to a COTS tag, but it has a limited sensing range, resolution, and robustness as mentioned in Section 1. It also incurs significant delay due to power sweep to get the threshold power in a commercial reader [26]. Our system uses a differential phase based metric to improve the accuracy and robustness. [43] develops a multiple tag system to detect the water level in a container using the ON-OFF switching. Researchers also exploit the impedance change in customized tags to sense on-body temperature [40, 44], relative humidity [45–47], and even gas leakage [48]. [39] proposes a specific patch-antenna design for temperature sensing. Unlike RTSense, these approaches require customized tags in a wired setup, making them relatively expensive and less practical. [49, 50] propose a few setup-independent metrics like Analog Identifier (AID) but is limited to sensing chemical presence and relative humidity [23]. Unlike these works, we propose a simple tag-pair design to exploit the antenna surface area for *analog sensing* of temperature and use differential phase sensing to improve the resolution, range, and robustness.

As shown in Table. 1, there are a few commercial RFID based temperature sensing technologies, such as [35, 37, 38]. They use chip (IC) impedance matching technology. While these tags [35] do not require an embedded battery, it is costly (*e.g.*, $50) due to its use of micro-controllers and memory for sensing purposes. [37] requires dedicated reader to read the information. In comparison, our technique supports commercial UHF tags (just augmented with copper foil). Moreover, these systems are not reliable in multi-path rich situations because the calibration method fails when the environment changes, whereas our differential sensing approach would work. There are also system-on-chip based approaches, such as [36], which embeds a temperature sensor into the tag and re-designs it completely. However, this dedicated approach makes the tag really costly and requires a dedicated reader setup. On the other hand, there is a recent work that uses high-bandwidth RFID tag antenna sensing to detect fake and real liquid [51]. This work deploys machine learning based approach to address environmental variations. Although this work is in the same space of tag antenna based sensing, it uses non-commercial USRP setup to perform binary classification. [52] modifies the IC architecture to sense temperature based on passive power. In comparison, our work uses commercial tags and readers and does not require complicated IC modification. Our loop tag combined with the copper dipole antenna also cost less (around $1.5). However, we require RFID reader/antenna (approximately 1200$ for multi-antenna solution and 600$ for single antenna solution), which is similar to [24].

3 PASSIVE RFID SYSTEM

A passive RFID system consists of a reader connected to the antenna(s) and battery-less passive tags. Passive RFID reader communicates with the tag through a back-scatter signal as depicted in Fig. 5. The reader sends a periodic continuous wave (CW) signal. The passive tags harvest energy from this CW signal and modulate its data on the back-scatter signals using ON-OFF keying.

3.1 Passive RFID reader

COTS passive RFID reader [26] uses linear or circular polarized antennas for both transmission and reception. They usually access lower level information [53] (*e.g.*, RSS and phase values using SDK [54]). A COTS reader employs an open or close loop estimation (*e.g.*, preamble correlation) to acquire the phase and RSS information.

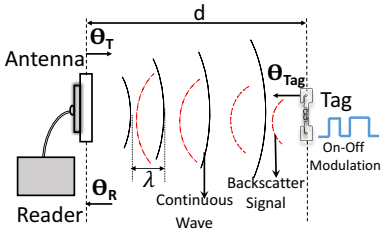

Figure 5: Operation of a reader, antenna and a tag.

3.2 Passive RFID tag

A typical chipped passive RFID tag consists of an antenna and an integrated circuit (chip). Passive RFID tag absorbs the most energy when the chip impedance (Z_C) and the antenna impedance (Z_A) are conjugately matched, *i.e.*, $Z_C = Z_A^*$ [55]. Specifically, the tag chip (IC) has two impedance states $Z_C(ON)$ and $Z_C(OFF)$. When the tag antenna switches to a well-matched state of $Z_C(ON)$, the reflection coefficient Γ_{ON} becomes close to zero. When the tag switches to $Z_C(OFF)$, it corresponds to a high reflection coefficient Γ_{OFF}, which is typically a shorted state where there is large impedance mismatch [56].

3.3 Passive RFID Tag Parameters

In the following, we provide a brief overview of RFID tag communication.

A. Tag Phase: Let d denote the distance between the reader antenna and tag. The signal traverses a total distance of $2d$ (Fig. 5) due to back-scatter. The phase not only changes with the distance, but also changes with the properties of transmitter antenna (θ_T), tag (θ_{TAG}), and receiver antenna (θ_R), where θ_{TAG} is a random offset and $\theta_T + \theta_R$ is a polarization offset that is determined by the location. $\theta_{TAG} + \theta_T + \theta_R$ can be considered as an initial phase offset.

The total phase change [57] observed by the reader can be expressed as:

$$\theta = (\frac{2\pi}{\lambda} \times 2d + \theta_T + \theta_{TAG} + \theta_R) \; mod \; 2\pi \tag{1}$$

where λ is the wavelength. $\theta_T + \theta_R$ can be expressed as polarization mismatch $2\phi(\hat{d})$. $\theta_{TAG} = arg(\frac{1}{Z_A+Z_C(OFF)} - \frac{1}{Z_A+Z_C(ON)})$. If we assume $Z_C(OFF) \rightarrow \infty$ (*i.e.*, practically very large) [23, 58], then the phase equation can be expressed as:

$$\theta = (\frac{2\pi}{\lambda} \times 2d + 2\phi(\hat{d}) + arg(-\frac{1}{Z_A + Z_C(ON)})) \; mod \; 2\pi \tag{2}$$

B. Tag Chip Threshold Power: Let P_{chip} denote the amount of harvested power transferred to the RFID chip (IC). P_{chip} is given by the following [22, 59, 60]:

$$P_{chip} = (1 - |\Gamma_{tag}|^2) G_{tag} G_t P_t \rho^2 (\frac{\lambda}{4\pi r})^2 \tag{3}$$

where r is the tag to reader distance, P_t is the reader antenna's transmission signal power, G_t is the gain of the reader antenna, G_{tag} is the gain of the tag antenna, λ is the wavelength of the signal, ρ is the polarization loss factor, which is a function of mis-match between the reader and the tag antennas. $\Gamma_{tag} = \frac{Z_C - Z_A^*}{Z_C + Z_A}$. Therefore, a change in the physical parameter (Λ) causes the minimum power required to power up the chip to change as follow:

$$P_{threshold} \propto (1 - |\Gamma_{tag}(\Lambda)|^2) G_{tag}(\Lambda) P_t \tag{4}$$

C. Tag Back-scattered Signal's Power Strength: Note that G_{tag}, Γ_{ON} and Γ_{OFF} are functions of Λ. Thus, the above equation can be expressed by including physical parameter of interest Λ [22, 56, 61]:

$$\delta P_{rec} = \frac{\lambda^4 G_t^2 G_{tag}(\Lambda)^2 P_t |\Gamma_{ON}(\Lambda) - \Gamma_{OFF}(\Lambda)|^2}{(4\pi r)^4} \tag{5}$$

4 MODEL-AIDED DESIGN OF RTSENSE

In this section, we introduce our RFID tag design and model that capture the impact of ambient temperature on the phase. We then use this model to develop RTSense to estimate the temperature in an environment-agnostic way based on the phase of the received signal. One of our major contributions is to identify the correct configuration and corresponding analytical model for R/L/C to match the measured impedance change. To the best of our knowledge, this is the first analytical model that captures the impact of temperature on a passive dipole based RFID.

To simplify our model, we design and build a simple antenna – a dipole antenna. The dipole antenna is a popular commercial RFID tag [62–64]. According to [65, 66], the basic design guideline for any chipped RFID tag antenna is size reduction without sacrificing the conjugate matching [22, 65]. We relax this requirement of size reduction for temperature sensing. We leverage the fact that the temperature changes the impedance of the tag, which in turn changes the phase of the back-scattered signal. We present the analytical model to show how the temperature changes the phase.

4.1 Mapping Temperature to Impedance

In RTSense, we leverage the observation that temperature variation changes the impedance in the tag-antenna. To understand how the impedance changes with the temperature, we need to know the electro-magnetic components of tag-dipole antennas and how they relate to the temperature.

4.1.1 Components of antenna. We use a simple dipole antenna design and leave a more sophisticated antenna design for future work. The dipole antenna has inductance L, resistance R, and capacitance C. Below we derive L, R, and C for a simple dipole antenna l long, w wide, and t thick when the RFID continuous-wave frequency is f and wave-length is λ.

According to [67], the inductance (L) of this antenna strip is:

$$L[nH] = 0.2l[mm][ln(\frac{2l}{w+t}) + 0.5 + \frac{w+t}{3l}] \tag{6}$$

The resistance (R) has two components: DC resistance from the intrinsic characteristic of the metal strip and AC resistance from the inductive coupling. The DC resistance of this strip is given by $\rho l/wt$, where ρ is the resistivity constant depending on the metal. For copper, $\rho = 1.68 \times 10^{-8}$. The AC resistance is given by $80\alpha^2(\frac{\pi l}{\lambda})^2$ [64, 68]. α depends on the current distribution along the dipole. The AC resistance depends upon the skin-depth, which increases with frequency [64, 69]. If the current distribution is triangular (*i.e.*, maximum at the center and zero at the ends), then

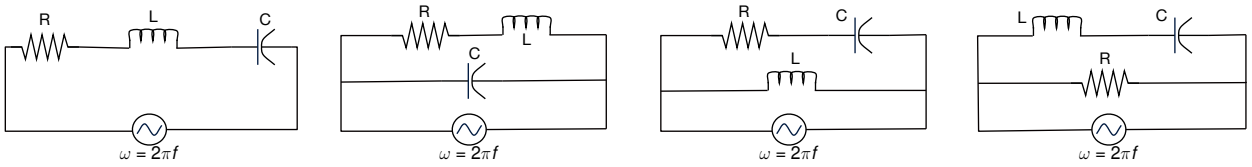

(a) Configuration 1 (C1). (b) Configuration 2 (C2). (c) Configuration 3 (C3). (d) Configuration 4 (C4).

(e) Configuration 5 (C5). (f) Configuration 6 (C6). (g) Configuration 7 (C7). (h) Configuration 8 (C8).

Figure 6: Possible configurations of a RFID tag antenna.

the value of α is chosen as 0.5. We use $\alpha = 0.5$ in our model. This can only happen if the length of the dipole is $\lambda/2$. We build our dipole to match this principle.

The capacitance (C) of the metal strip is given by $C = wt\epsilon/d$, where d is the distance between two halves of the dipole antenna. We get these initial components (R, L, and C) using these analytical models, and verify using both Ansys HFSS software [70] and LCR meter [71]. We observe that our analytical model matches closely with the simulation in HFSS and LCR meter values.

4.1.2 Modeling the Impedance. How the impedance relates to the L, R, C depends on the circuit configuration. Although some existing works [72, 73] assumes a simple series R-L-C model like Fig. 6(a), we find that it is not accurate. For a given frequency f, we measure the impedance of the RFID tag using Array Solutions Vector Network Analyzer (VNA) [74]. We observe that the real components of the measured impedance vector change across different samples at a fixed temperature. We create all 8 possible configurations as shown in Fig. 6. We compare the impedance measured using VNA with the impedance derived by plugging the L, R, C measured using the LCR meter [71] to each of the 8 configurations. Then we select the configuration that best approximates the measurement. This configuration selection is critical for our modeling.

Fig. 7 shows the average error of impedance magnitude across all configurations in Fig. 6 as we vary the copper dipole antennas' area and length. As the figure shows, the configuration 2 yields the lowest error. This is also consistent with a few recent works [62, 75]. Therefore, we use this configuration to model the impedance of dipole antenna. In this configuration, the equivalent impedance relates to R, L, and C as follow:

$$Z_{eq} = \frac{R}{1+\omega^2(R^2C^2-2LC)+\omega^4L^2C^2} + j\frac{\omega(L-R^2C)-\omega^3L^2C}{1+\omega^2(R^2C^2-2LC)+\omega^4L^2C^2} \quad (7)$$

4.1.3 Temperature impact on impedance. Next we analyze the impact of temperature change on the impedance. The resistance relates to the temperature as follows [69]:

$$R_T = R(1 + \alpha(T - T_0)) \quad (8)$$

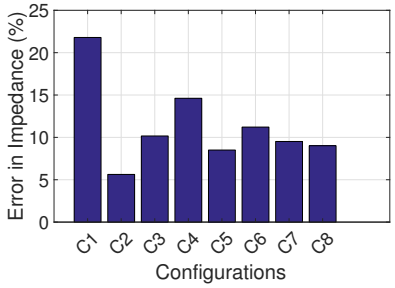

Figure 7: Average percentage error in impedance magnitude among different configurations in Fig. 6.

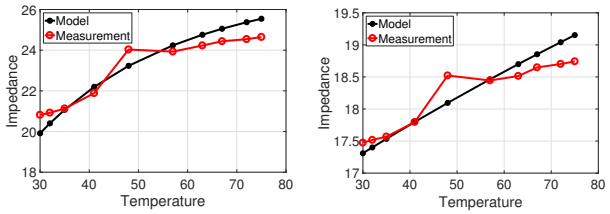

(a) Larger Width (30cm). (b) Smaller Width (5cm).

Figure 8: Impedance prediction (Model vs VNA). A larger width has higher impedance magnitude (20) than that of a smaller width (17.5). Here, temperature is in ° Celsius.

where R_T is the resistance at temperature T, T_0 is the room temperature, and α is the temperature coefficient of resistance change. We choose copper for our dipole antenna design. α is 0.004041 for copper.

The relationship between the inductance and temperature is given by the following equation:

$$L_T = \frac{1}{2\pi f w}\sqrt{\pi f \mu_0 \rho}\sqrt{1 + \gamma(T - T_0)} \quad (9)$$

where μ_0 is the magnetic permeability, $\gamma = 0.0034$ per centigrade, and T_0 is considered as the standard room temperature.

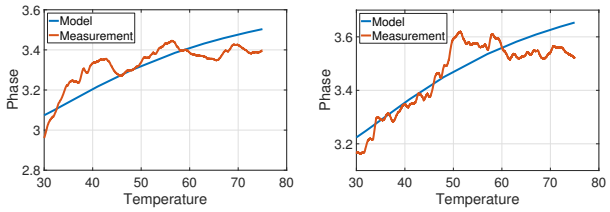

(a) Location 1. (b) Location 2.

Figure 9: Modeling phase change with temperature for a 5cm wide antenna. Temperature is in ° Celsius.

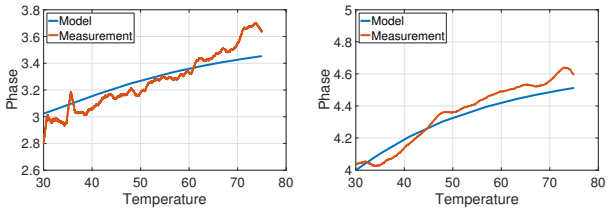

(a) Location 1. (b) Location 2.

Figure 10: Modeling phase change with temperature for a 30cm wide antenna. Temperature is in ° Celsius.

In the temperature range, we are interested in, the change in the capacitance of a metal strip is negligible [69].

Therefore, for a given temperature change, we first compute the new resistance and inductance, and plug them into Equation 7 to derive the resulting impedance. As shown in Fig. 8, our model and measurement match closely for different antenna dimensions. The impedance changes with $R/L/C$, and the amount of $R/L/C$ change varies with the antenna size. This insight motivates us to adjust the antenna surface area for differential sensing purposes.

4.2 Mapping Impedance to Phase

Next we map this impedance change to the phase change. Note that the tag antenna's impedance Z_A is a function of the temperature Λ. Using the equation Eq. 2 in Sec. 3, we have:

$$\theta = \left(\frac{2\pi}{\lambda} \times 2d + 2\phi(\hat{d}) + arg\left(-\frac{1}{Z_A(\Lambda)+Z_C(ON)}\right) \right) \ mod\ 2\pi$$

As shown in the above equation, the tag antenna impedance, tag to reader antenna distance, and polarization mismatch (due to tag orientation) all affect the phase of the signal arriving at the reader. Suppose the antenna impedance only changes with the temperature of Λ, which can be achieved by selecting an appropriate material sensitive to only the temperature change but not other environmental factors. Then we can relate the phase change with the temperature change as follows:

$$\theta_{Diff.} = arg\left(-\frac{1}{Z_A(\Lambda)+Z_C(ON)}\right) - arg\left(-\frac{1}{Z_A(\Lambda_{ref})+Z_C(ON)}\right) \quad (10)$$

where $Z_A(\Lambda_{ref})$ and $Z_A(\Lambda)$ are the impedance at the reference temperature Λ_{ref} and current temperature Λ.

We experiment with a small distance to minimize all other factors except the temperature in an iso-temperature oven (described in the setup later in Sec. 6). We measure the phase using copper dipole tags with 5 cm and 30 cm wide antennas at two different distances: 10 cm and 15 cm. As shown in Fig 9 and Fig. 10, the estimated phase change using Equation 10 matches closely with the phase measurement. All these measured trends are the average of 5 sample runs at each location and the mean error range at each point is approximately 0.02 radian. While there is a small variation due to multi-path, the trends, and range of the change match quite well. Note that the fit is better in the 30 cm tag than the 5 cm tag, likely because the larger tag yields a stronger signal and cleaner phase measurement. Overall the results validate our model. Therefore, in the absence of multi-path, we can map the measured phase change to the temperature change using our model.

4.3 Phase Difference Metric of RTSense

In practice, many other factors can change the phase of the received signal besides the temperature. To improve robustness against the changes from other environmental factors, such as motion and multi-path, we make the following observations from the above model. The absolute metrics, including raw phase, power threshold, or received signal strength (RSS) are setup-dependent and hard to use for general sensing. This has also been reported in a few recent works [25, 49, 64].

Instead, differential sensing, which takes the difference between the two antennas is relatively more robust. However, power-based metrics (*e.g.*, RSS, or minimum threshold power) depend on many factors, such as antenna gains, transmitted power resolution, and power transfer coefficients, as shown in Eq. 10 and Eq. 4. Moreover, to get the power threshold, we need to perform a power sweep and the change allowed is coarse – around 0.3 dBm [24], which limits the resolution of power-based temperature sensing. Therefore we adopt the differential phase-based sensing. For the difference, we seek two tags that change differently with the temperature.

As shown in Fig. 8, dipole antennas with different sizes respond differently to the same temperature change. Therefore we can use two tags with different sizes and map the difference in their phase change to the temperature change. $Z_C(ON)$ is equal in both tags since the same RFID chip/transponder is used. We put these two tags next to each other.We then take difference between the two tag signals. We create the signal vector for the back-scattered signal and derive RSS A and phase ϕ as $A\exp^{j\phi}$. This vector difference eliminates the background multi-path signal. We collect these phase-vector differences and unwrap to estimate the temperature.

5 RTSENSE: SYSTEM DESIGN

In this section, we introduce our system, RTSense. It consists of two stages: the calibration stage and the estimation stage.

Calibration stage: The initial calibration step is performed during the installation time. It is a simple low-cost step to record the phase difference at the reader. During this step, Impinj R420 RFID reader continuously reads the tag-pair at a rate of 200 reads/second, and records the phases of all back-scatter responses. Note that this is one-time effort and does not need to be repeated even when the tag orientation or distance changes. RTSense *normalizes* the phase-difference (after unwrapping them) with respect to the lowest value:

$$p(x) = r(x) - \min_x r(x), \quad T_{min} \le x \le T_{max} \quad (11)$$

where $r(x)$ is the (unwrapped) raw phase difference at temperature T, which changes from T_{min} to T_{max}. We calculate the normalized $r_{TagBig} - r_{TagSmall}$ during the calibration step. The temperature and phase are measured after installing the copper tag-pair with a ground plane. RTSense then uses polynomial curve-fitting to find the *third-order* polynomial that best fits the normalized calibration data. This calibrated polynomial is used for temperature estimation even if the location or orientation of the tag-pair and RFID antenna changes. We apply the model calibrated using the data collected from a lab to the measurement collected in a conference room, and observe 0.9-degree increase in the median error. This suggests that calibration can potentially be done once and used later in an environment-independent way. To improve the temperature estimation accuracy through diversity, we extend our system to use three antennas 1m apart to estimate the temperature. We aggregate the estimations using a weighted average and we call this approach RTSense (Multi).

To exploit frequency diversity (called RTSense (FD)) with multiple antennas, we calibrate $p(x)$ using 30 channels ranging from 860 MHz to 920 MHz (2 MHz apart). We use USRP N2100 with SBX daughter-board. We capture the I/Q samples from the USRP to extract the relevant RF parameters. We use these calibrated polynomials to estimate the temperature and aggregate the estimations using a weighted average.

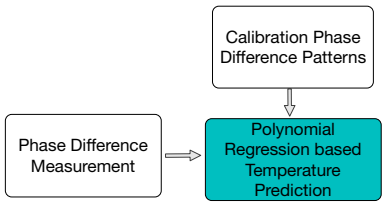

Figure 11: Algorithmic overview of RTSense.

Estimation stage: At the estimation stage, we use the newly measured phase difference to estimate the temperature as shown in Fig. 11. We record the phase difference during 10 seconds and take an average. Then we put this average phase difference in the previously calibrated polynomial regression model to estimate the temperature. We can further leverage frequency diversity to calibrate and estimate for each frequency and combine the estimation results to improve the accuracy. We combine estimations from multiple frequencies using the weighted average, where the weights are inversely proportional to the RSS variation. A similar combination strategy is used to leverage MIMO diversity [76]. We combine estimations from multiple antennas in the same way. We further compare with other combining schemes in Fig. 21.

6 EVALUATION METHODOLOGIES

In this section, we first describe experimental setups used to validate various observations, which are critical in building the *end-to-end* system. We then introduce other methodologies for RFID-based temperature sensing for comparison.

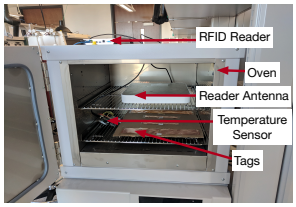

(a) Oven experiment.

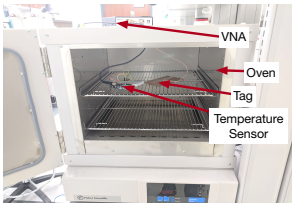

(b) Oven experiment with VNA.

Figure 12: Iso-temperature oven experiment setup.

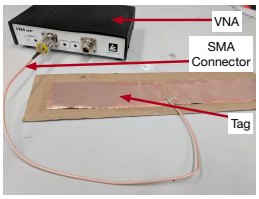

(a) VNA Setup.

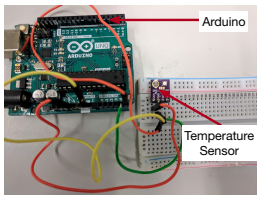

(b) Temperature Setup.

Figure 13: Different setup components.

6.1 Setup

Oven Setup: We use a Fisher Scientific iso-temperature oven [77] to control the temperate as shown in Fig. 12. This oven gives us the flexibility to keep the temperature the same throughout the whole setup. We connect the 0.01 inch thick copper dipole antennas to the Vector Network Analyzer (VNA) [74] using the SMA connector (Fig. 13(a)) and use it inside the oven for evaluation. Fig. 12 shows the experimental setup inside the oven and how the VNA is connected. We use an Arduino [78] based temperature sensor Fig. 13(b)) [79] to record the ground-truth temperature for quantifying our estimation error. We change the temperature from 15° to 85° centigrade in our experiments, which covers our use-cases. The temperature readings are synchronized with the reader software and VNA through a laptop.

Lab Setup: We also perform experiments using four different types of COTS UHF tags in the same oven setup. The tags are Alien-9654 Higgs 3 (Tag1), Smartrac Frog-3D (Tag2), Alien-9640 Higgs-3 (Tag3), and Alien-9768 Higgs 4 (Tag4) [80]. We measure the ground-truth L-C-R through an LCR meter [71] to compare our analytical model with Ansys HFSS software-based model. We perform different experiments by changing the distance and orientation. We use a heat-gun in a cardboard setup as shown in Fig. 14. We use the temperature sensor in tandem to record the ground-truth, and use the cardboard box to help maintain the temperature constant in the setup. We change the temperature from 15° to 85° centigrade. We also perform micro-benchmark experiments by changing the orientation and distance in this setup. Like the previous setup, the RFID reader and temperature sensor are both connected and synchronized through a laptop. To support multiple frequencies, we also use USRP N2100 [81] with SBX daughter-board [82] and two antennas as a reader, as shown in Fig. 15.

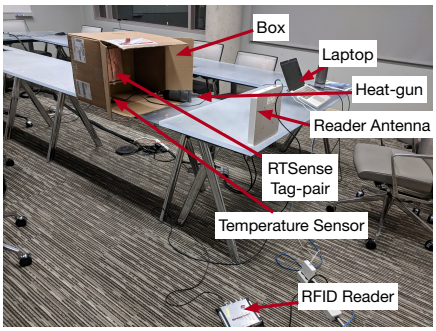

Figure 14: Experimental setup with a heat-gun in a room.

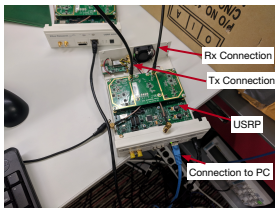

(a) USRP SBX Connection.

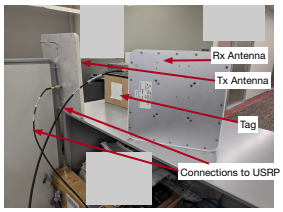

(b) USRP Antennas and Tag.

Figure 15: USRP Setup for RTSense (FD).

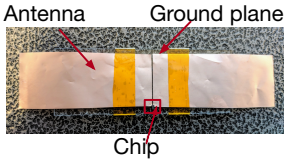

(a) Tag Design Type 1

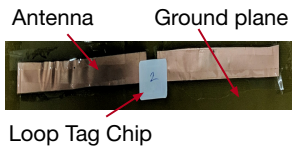

(b) Tag Design Type 2

Figure 16: Two types of tag design.

Tag Design: Fig. 16 shows two possible designs of customized copper tags in RTSense. We create chipped passive RFID tags with a simple copper dipole antenna. In one design, shown in Fig. 16(a), we use the off-the-shelf transponder and carefully solder with the tag antennas. We connect two transponder connections to separate dipole arms of the antenna without shorting them for successful communication with the COTS reader. In an alternative design, shown in Fig. 16(b), we use a smaller loop chipped tag (Alien-9613 Higgs-3) as the communicating element while attaching it to two separate dipole arms. This design is used to simplify customized RFID tags for sensing purposes. Unless otherwise specified, we use this tag-pair design (Fig. 16(b)) for experiments. Our tag-pair costs around $1.5: a few cents for tags and around $1.5 for the foil.

6.2 Other Methods of Temperature Sensing

In this subsection, we describe other sensing techniques. Although these techniques are not designed for temperature sensing, we adapt them for comparison.

AID: [23, 50] proposes the Analog Identifier (AID) to sense moisture. AID combines the direct and reverse link power parameters to eliminate the environmental influence. It is given by:

$$AID = \frac{p_c}{2\sqrt{P_{R\leftarrow T}P_{threshold}}} = \alpha R_C \mid \frac{1}{Z_A + Z_C} \mid \quad (12)$$

where p_c is the chip sensitivity, *i.e.*, minimum amount of power (in dB) required to power up the chip, which can be procured from the data-sheet, and $P_{R\leftarrow T}$ (Eq. 5) is the back-scattered signal strength. However, AID has limited resolution since it depends on $P_{threshold}$ (Eq. 4), which can only be adjusted in 0.3 dBm.

Single tag phase difference (PD): [49] uses the phase difference to sense moisture. Specifically, it defines $\Delta\phi(t) = \phi(t) - \phi(0)$, where $\phi(0)$ is the reference state. Phase based sensing has the potential to achieve better resolution than power-based sensing but is sensitive to multi-path. Our work uses the phase difference to sense the temperature and addresses the multi-path issue by taking the difference between two co-located antennas.

Differential Minimum Threshold Power (DMRT): Recently [24] adds a sensor to a commercial UHF tag-pair. It calculates $P_{threshold}(A) - P_{threshold}(B)$(Eq. 4) where the tag A is the instrumented tag and the tag B is not. Since it is a power-based technique like AID, its resolution is limited.

7 IMPLEMENTATION DETAILS

Next, we describe the implementation detail of the tag designs and the hardware used in RTSense. The RFID setup used in RTSense consists of an ETSI-based Impinj R420 reader, which continuously queries the tag-pair in the range at around 200 reads/second using circular polarized antennas with 9dBi gain [83]. We use 867.5MHz for our experiments and record the responses of the tags at different temperature levels in both the oven and heating gun setup. Apart from this basic COTS reader setup, we implement a software-based RFID reader [84] in USRP N2100 [81] with a SBX daughter-board [82] with two circularly polarized antennas (in GNURadio v3.74). Then we collect the I/Q samples of the reflected signal from the tag to extract the RSS and phase of the signal. The USRP is necessary to support higher bandwidth (*e.g.*, 860 MHz to 920 MHz) to achieve higher accuracy. We also use the Vector Network Analyzer (VNA) of Array Solutions, which sweeps up to 1GHz to measure the impedance of the antennas. The VNA is connected to the copper dipole antenna with an SMA connector, as shown in Fig. 13(a). We record the impedance components via the the connected laptop.

Apart from the tag and transponder used in RTSense, we also use commercial RFID tags as shown in Fig. 17. It operates between 860−920 MHz. These tags include different types of dipole antennas, such as clover-leaf, tip-load, T-match, and spiral shape. For AID and DMRT, we change different power levels using LLRP protocol through JAVA sdk in Impinj Reader and record the RF phase and RSS in all responses. In our frequency diversity approach, we employ the frequency sweep of 80 MHz through a USRP based implementation. We use 0.02 inch thick copper [85, 86] with a particular RFID transponder [87] and the ground-plane of FR4 substrate [88]. We use Fisher Scientific's iso-temperature oven [77] in our experiments

and an Arduino-based [78] temperature sensor [79] in Fig. 13(b) to record the ground-truth temperature to quantify the sensing error. This temperature sensor module [79] has 0.5° C accuracy. We use a Macbook Pro running OS Sierra with a 8GB RAM, and i5 quad-core processor to process the data. We also try processing the data on Raspberry Pi 3 Model B [89] with 1.2 GHz quad-core broadcom processor and 1 GB RAM. It takes around 1 second on the laptop and 6.5 second on the Raspberry Pi 3 to process the data and estimate the temperature. Both processing speeds are adequate for real-time monitoring.

8 EVALUATION

We perform extensive experiments to evaluate RTSense. Initially, we start with the basic observation of phase change with the temperature in both COTS UHF tags and custom-designed copper-based dipole tags and justify the design choice. We show a simple copper-dipole-based tag-pair design can open up an interesting sensing opportunity. Next, we compare phase-based sensing with other power-driven methods. We also show that multiple antennas and frequency diversity also help improve sensing accuracy. Next, we perform some micro-benchmark experiments by changing the multi-path setting, distance, area of the tag antenna, and orientation of the tag-pair relative to the RFID antenna setup. We also show the performance of alternative curve-fitting based techniques in the estimation stage of RTSense.

8.1 Rationale behind tag-pair design

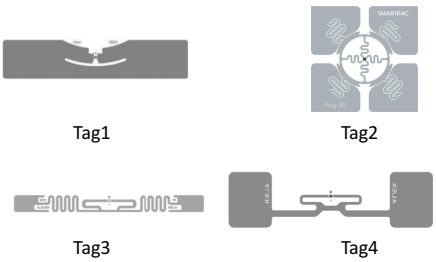

Figure 17: Types of COTS UHF tags used.

Why not COTS UHF Tags? We start with COTS UHF RFID tags with different types of dipole antenna design as shown in Fig. 17. Fig. 18 shows the phase change for the four types of tags when we vary the temperature. As we can see, the phase does not change monotonically (except Tag1, which has a simple dipole design. We do not select Tag1 since its phase resolution is coarse – only 0.4 radian and it is not easy to adjust the resolution. In comparison, in the copper dipole based approach, we can change the width of the antenna size easily to adjust the resolution.). The non-monotonic phase change is primarily due to the complex antenna-design artifacts, which cause polarization mismatch and mutual coupling between tag antenna elements [65]. If one looks carefully at Fig. 18, one can find out more variation in phase-change patterns in *Tag2* and *Tag3*. This happens due to their folded-dipole design, which influences two electro-magnetic fields, and spiral-design with T-match loading, which causes non-uniform current distribution [63, 68]. Since it is hard to modify antenna design and material used in COTS UHF tags through fabrication, we choose to attach a rectangular dipole antenna to COTS loop tags due to minimum modification. Therefore, the fundamental reason behind this behavior is the shape and material used in COTS UHF tags. Furthermore, because of this non-monotonic non-uniform behavior, the phase difference metric between two different UHF tags with different areas will not yield good results.

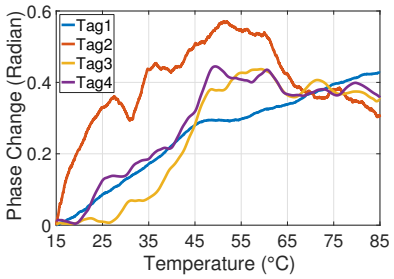

Figure 18: Single COTS UHF tag phase change pattern. Experiments are performed in the oven.

Why area-based tag pair? We use a simpler antenna design (*i.e.*, dipole antenna) with a widely-available copper. Our model suggests that under the same temperature change a larger antenna results in larger impedance change, and thus more phase variation. To further confirm this insight, we perform an experiment by changing the antenna surface area of copper dipole tag from 2cm to 30cm while fixing the dipole length constant (17.30cm), which is equivalent to half the wavelength according to [64, 65, 68]). Fig. 19 shows a larger surface area yields a larger phase change. For example, 70-degree celsius change results in 1.7 radian phase change in a 30cm wide dipole antenna, but only 0.3 radian phase change in 2 cm wide antenna. Therefore, a larger copper dipole-antenna-based tag provides better resolution and higher accuracy in temperature sensing. We use a tag-pair to cancel out the impact of other environmental factors.

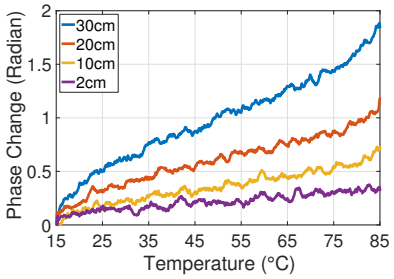

Figure 19: Phase change pattern of custom-designed tags with different areas. Experiments are done in an oven.

Fig. 19 shows the phase changes increases with the antenna size. Fig. 20 shows that changing the temperature from 15 degree celsius to 85 degree celsius results in 1.32 radian phase difference in the 30cm-2cm tag-pair, but only results in 0.3 radian phase change in the 10cm-2cm tag-pair. We add the chip to this tag-pair design by

attaching either a chip transponder or smaller loop tags as explained earlier. This also makes the design process simple. Note that we do not go beyond the 30cm area since exceeding 30 cm will result in detuning. To reduce the surface area in certain applications, one can *fold* the copper to reduce the area. But this has to be done carefully to take into account the potential mutual coupling.

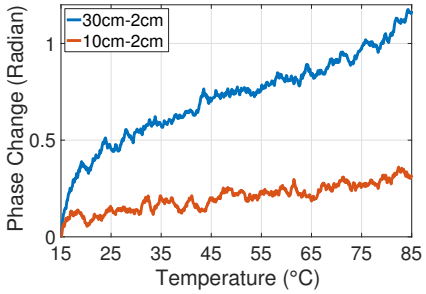

Figure 20: Phase change pattern of a pair of custom-designed copper tags with different areas in the oven.

8.2 Comparison with Other Methodologies

In this subsection, we compare RTSense with other methodologies mentioned earlier. Before comparing with other methodologies, We first evaluate RTSense (FD), which uses multiple frequencies. In Fig. 21, we combine the temperature estimations from different frequencies using the following schemes: (i) assigning weights inversely proportionally to the signal strength variation at a given temperature, (ii) assigning equal weights to all frequencies, and (iii) selecting the maximum or minimum of the temperature estimations across frequencies. In all the schemes, weights are normalized such that the weights sum up to 1 across all frequencies. As we can see from Fig. 22, (i) performs the best and yields around 2.9° centigrade median error.

Unless specified, the other schemes use the antennas of the same size. Fig. 22 shows that RTSense performs better than the other schemes. We perform the temperature experiments using a heating-gun from 200cm away. The median error of RTSense using one antenna is around 6°. Using 3 antennas (1 m apart [1]) reduces the median error to around 4° (RTSense (Multi)). Using 60 MHz bandwidth (consisting of 30 channels 2 MHz apart) and 3 antennas (RTSense (FD)) further reduces the error to 2.9° celsius by exploiting the frequency diversity. In comparison, AID and DMRT yield around 24°, which is consistent with the 20 degree resolution and 32° error reported by the authors of AID and DMRT. Moreover, the power changes non-monotonically with the temperature as shown in Fig. 24. Fig. 23 further illustrates that both RTSense (FD) and RTSense (Multi) perform similarly across difference temperature.

In addition, the power-based schemes degrade if there is a minor change in the setup due to the multi-path and lower resolution of the power level of commercial devices. According to the Eq. 4, power is a non-linear function of many factors, including the gain of tag-antenna and transmit power, etc. Furthermore, this moderate resolution is also due to the coarse power resolution. In our case, it is 0.25dBm in Impinj RFID reader.

[1]We have also tested using over 1m separation and have not seen better performance.

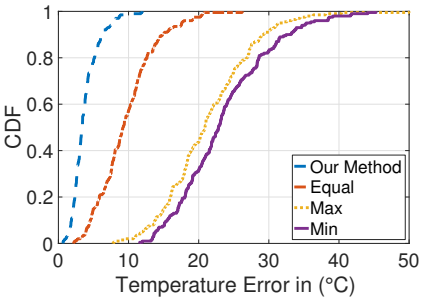

Figure 21: Temperature estimation error with different strategies in RTSense (FD).

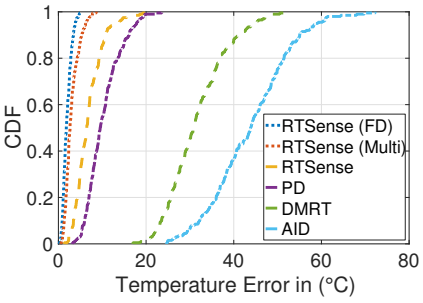

Figure 22: Temperature estimation error with different strategies compared to RTSense (FD).

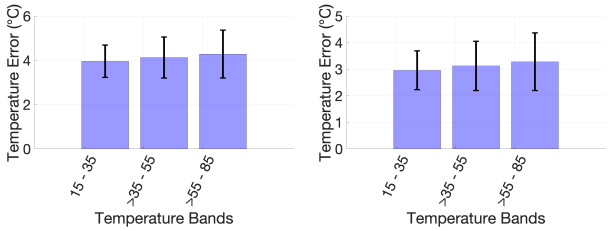

(a) RTSense (FD). (b) RTSense (Multi).

Figure 23: Temperature sensing error using RTSense (FD) and RTSense (Multi) under different temperature.

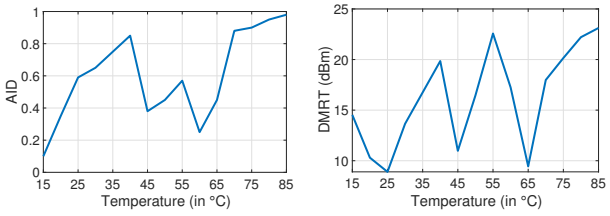

(a) AID example. (b) DMRT example.

Figure 24: Example patterns with temperature change.

The range of DMRT or AID based metric is limited. For these two methods, we only report the error up to 1.5m distance, which is the maximum range we can collect the data. DMRT is not easy to repeat since it is sensitive to the multi-path. Adding a sensor to the tag

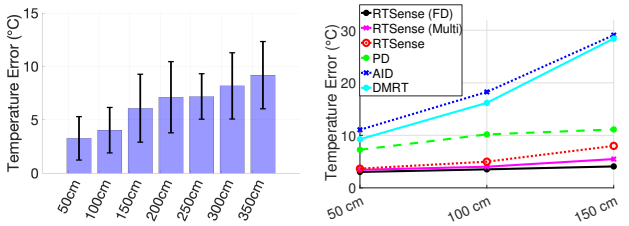

(a) Distance change. (b) Different schemes.

Figure 25: Temperature estimation error with distance change. Experiments are performed using the heat-gun setup.

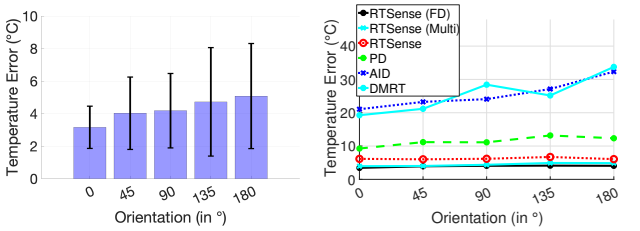

(a) Orientation change. (b) Different schemes.

Figure 26: Temperature estimation error under different orientation. Experiments are performed using the heat-gun setup.

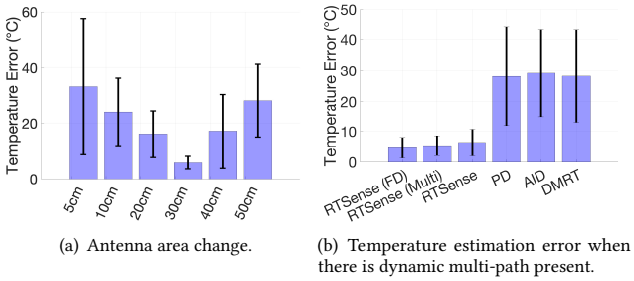

(a) Antenna area change. (b) Temperature estimation error when there is dynamic multi-path present.

Figure 27: Temperature estimation error after changing the antenna area and dynamic multi-path. Experiments are performed in the heat-gun setup.

also detunes the tag heavily and the impact is amplified when the temperature changes, which may cause failures in reading the tag. AID has limited accuracy due to the coarse resolution of received signal strength and $P_{threshold}$. Furthermore, performing a sweep across different power levels is time-consuming. For example, it takes several minutes to sweep all power levels for our reader.

In comparison, the phase-based method performs better in terms of range, resolution, robustness, and delay. RTSense works up to 3.5m range, even in non-line-of-sight. Interestingly, other phase-based technique (namely *PD*) also out-performs the power-based approach. As shown in Fig. 22, *PD* yields a median error of 10° centigrade since it is sensitive to other environmental change due to the lack of differential sensing approach.

8.3 Micro-benchmark Experiments

In this subsection, we perform different micro-benchmark experiments by changing the tag orientation, tag to antenna distance, and antenna surface area. We also change the static multi-path by moving the furniture around and perform experiments in different locations.

Impact of Distance: We first evaluate the impact of the distance on RTSense. We change the distance of the antenna from 50cm to 350cm. We calibrate the phase-difference trend at 50cm distance. Fig. 25(a) shows that although the temperature estimation error increases slightly with the distance, but the median error remains within 7.5° error even when it is 3.5m away. We also compared with other techniques within the 1.5m range due to the range limitation in the power-based schemes and observe that RTSense performs the best as shown in Fig. 25(b). The error in AID or DMRT can go up to around 30° centigrade. We can further increase the sensing range by using a higher gain antenna or MIMO technique (*e.g.*, beam-forming [90]).

Impact of Orientation: Next we change the tag orientation from 0° to 180° on a single plane, as shown in Fig. 26(b). Since we use the tag-pair based approach in RTSense, the polarization mismatch due to different orientations cancels out. Therefore, we observe a similar error range at different orientations for RTSense as shown in Fig. 26(a). Fig. 26(b) shows that the single-tag-based techniques like *PD* or *AID* suffer significantly from polarization mismatch and their errors can go beyond 30° centigrade. In this experiment, we perform calibration at 100cm distance with 0° orientation and measure at 100cm distance.

Impact of Antenna Area Change: In this experiment, we perform calibration at 100cm away with 0° orientation and measure at 100cm away while changing the temperature. We change the surface area of the larger tag-antenna from 5cm to 50cm. As shown in Fig. 27(a), 30cm is the optimal in our copper-dipole tag-pair based setup with the COTS chips. Note that the performance does not monotonically increase with the antenna size since while increasing the antenna size increases the phase difference between the two antennas but it can cause antenna and tag chip impedance mismatch, which can degrade the accuracy. 30 cm provides a good trade-off between these two factors.

Impact of Calibration Location: To evaluate the dependence of location in the calibration stage, we perform the calibration from the data collected at a conference room and perform the estimation in two other rooms and vice versa. One room is a lab and the other room is an apartment. For these experiments, we have collected 5 sample runs at 5 different distances starting from 50cm and ranging upto 350cm. However, we did not change the antenna orientation for these experiments. Fig. 28 illustrates that the median temperature estimation error and overall trend remain similar. The median estimation error worsens approximately 0.9 degree when the location is different during calibration and estimation stages.

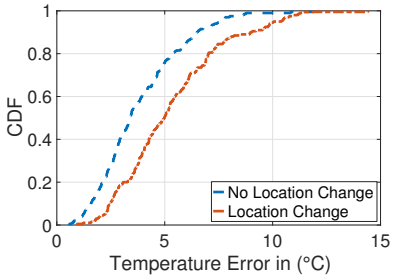

Figure 28: CDF of temperature estimation error in RTSense(FD). We perform calibration first at the same location and then at a different location.

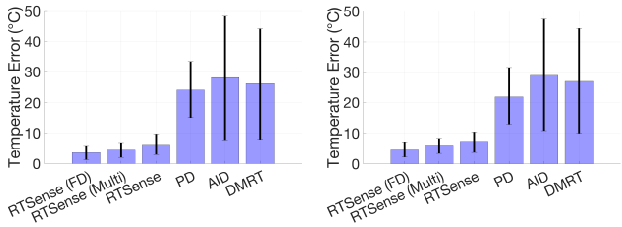

(a) Location 1. (b) Location 2.

Figure 29: Temperature estimation error at two different locations. We further change the multipath by rearranging the furniture. Experiments are performed using the heat-gun setup.

Impact of Multi-path: To observe the multi-path effect, we evaluate in two different rooms. We observe that the error is in the same region as shown in Fig. 29. We also re-organize the furniture in each room across different runs to change the static multi-path. Even if the calibration and estimation distance remains the same, the phase-based schemes perform better than the power-based schemes. Fig. 29(a) shows that when we change the static multi-path, the median temperature estimation error in *PD* increases up to 24° centigrade, but the error of RTSense, RTSense (Multi) and RTSense (FD) remain around 6° centigrade (C), 5° C, and 4° C, respectively. The power-based temperature estimation techniques suffer as shown in Fig. 29(a) and Fig. 29(b). In these experiments, we perform calibration at 150cm away with 0° orientation and measure at 150cm distance.

Furthermore, in the bigger room, we create a dynamic multi-path by having a user move around and occasionally block the line-of-sight path. Fig. 27(b) shows that *PD* has around 30° C mean error while RTSense (FD), RTSense (Multi), and RTSense have around 4°, 5°, and 6° C mean errors, respectively.

8.4 Impact of Fitting Functions

In this section, we examine a few simple alternatives in the estimation stage of RTSense. We conduct measurement in a conference room using the heating gun setup. We measure from 200cm away. We fit the measured phase difference and temperature using polynomial regression (PR) with degree 3. Table 2 shows the results of other regression. In all cases, we use the data collected from the ground-truth temperature. As we can see, the 3rd-degree polynomial regression provides the best performance: its median error is 6.12° centigrade using narrow-band frequency; increasing the bandwidth to 30 channels reduces the error to 3.8° C; increasing the antennas to 3 reduces the error to 4.2° C; using both high bandwidth and 3 antennas results in the lowest error of 2.9° C. Linear regression does not work well since the data is inherently non-linear. Using a too high order polynomial increases the error due to over-fitting.

Technique	Median Error (°C)
LR	18.34
LR with Regularization	18.38
PR with Degree 2	8.13
PR with Degree 3	**6.12**
PR with Degree 3 (3 antennas)	**3.8**
PR with Degree 3 (with 60 MHz)	**4.2**
PR with Degree 3 (multiple with 60 MHz)	**2.9**
PR with Degree 4	7.29
PR with Degree 5	8.39

Table 2: Error in RTSense with Other Techniques.

9 CONCLUSION AND FUTURE WORKS

In this paper, we develop an analytical model to understand how impedance and phase change with the temperature. Based on the model, we design a novel approach that uses phase to sense the temperature. We implement a customized tag-pair and measure the phase difference of the received signals from two tags with different sizes to estimate the temperature change. Our extensive evaluation shows the promise of our approach.

As part of the future work, it will be interesting to explore antenna and custom chip design to further improve the accuracy. In particular, we start with a simple dipole antenna design in RTSense to simplify our model. We would like to explore other antenna designs and understand their impact on the performance. Patch-based antennas, clover-leaf antenna, inverse-F antenna [65] may be worth considering. Moreover, we start with the temperature sensing in RTSense using copper tag-pairs, we would like to extend to sensing other properties such as humidity and light, etc. This can be achieved by selecting an appropriate material that is sensitive to the physical property being sensed. Moreover, it would be interesting to further evaluate and enhance robustness against different environments.

10 ACKNOWLEDGMENTS

This work is supported in part by NSF Grant CNS-1718585. We are grateful to the anonymous reviewers and the shepherd for their insightful comments and suggestions.

REFERENCES

[1] "What's the difference between temperature-controlled and climate- controlled storage?." https://bit.ly/2XDkYdA.

[2] C.-S. Pan, H.-C. Chiang, M.-C. Yen, and C.-C. Wang, "Thermal comfort and energy saving of a personalized pfcu air-conditioning system," *Energy and Buildings*, vol. 37, pp. 443–449, 05 2005.

[3] J. F. Nicol and M. A. Humphreys, "Adaptive thermal comfort and sustainable thermal standards for buildings," 2001.

[4] "The effects of high and low ambient temperatures on human sleep stages," *Electroencephalography and Clinical Neurophysiology*, vol. 51, no. 5, pp. 494 – 501, 1981.

[5] V. Gupta, S. Mittal, S. Bhaumik, and R. Roy, "Assisting humans to achieve optimal sleep by changing ambient temperature," in *2016 IEEE International Conference on Bioinformatics and Biomedicine (BIBM)*, pp. 841–845, Dec 2016.

[6] "The indoor generation and the health risks of spending more time inside." https://bit.ly/2XR7FUs.

[7] "Selling temperature-sensitive products? you need temperature-controlled warehousing." https://www.shipbob.com/blog/temperature-controlled-warehousing/.

[8] G. V. Angelov, D. P. Nikolakov, I. N. Ruskova, E. E. Gieva, and M. L. Spasova, *Healthcare Sensing and Monitoring*, pp. 226–262. Cham: Springer International Publishing, 2019.

[9] D. Roberts and K. Lay, "Variability in measured space temperatures in 60 homes," 2013.

[10] J. Kreider, *Handbook of Heating, Ventilation, and Air Conditioning*. Handbook Series for Mechanical Engineering, Taylor & Francis, 2001.

[11] "Smt160: Smartec temperature sensor." https://bit.ly/3fku0C2.

[12] A. P. Sample, D. J. Yeager, P. S. Powledge, and J. R. Smith, "Design of a passively-powered, programmable sensing platform for uhf rfid systems," in *2007 IEEE International Conference on RFID*, pp. 149–156, March 2007.

[13] N. Fasarakis-Hilliard, P. N. Alevizos, and A. Bletsas, "Coherent detection and channel coding for bistatic scatter radio sensor networking," *2015 IEEE International Conference on Communications (ICC)*, pp. 4895–4900, 2015.

[14] J. Fernández-Salmerón, A. Rivandeneyra, F. Martínez-Martí, L. F. Capitán-Vallvey, A. J. Palma, and M. A. Carvajal, "Passive uhf rfid tag with multiple sensing capabilities," in *Sensors*, 2015.

[15] R. Bhattacharyya, C. Floerkemeier, and S. E. Sarma, "Rfid tag antenna based temperature sensing," *2010 IEEE International Conference on RFID (IEEE RFID 2010)*, pp. 8–15, 2010.

[16] J. Wang, D. Vasisht, and D. Katabi, "Rf-idraw: Virtual touch screen in the air using rf signals," in *Proceedings of the 2014 ACM Conference on SIGCOMM*, SIGCOMM '14, (New York, NY, USA), pp. 235–246, ACM, 2014.

[17] L. Shangguan and K. Jamieson, "Leveraging electromagnetic polarization in a two-antenna motion tracking system," *ACM CoNext*, 2016.

[18] H. Ding, L. Shangguan, Z. Yang, J. Han, Z. Zhou, P. Yang, W. Xi, and J. Zhao, "Femo: A platform for free-weight exercise monitoring with rfids," in *Proceedings of the 13th ACM Conference on Embedded Networked Sensor Systems*, SenSys '15, (New York, NY, USA), pp. 141–154, ACM, 2015.

[19] L. Shangguan, Z. Zhou, X. Zheng, L. Yang, Y. Liu, and J. Han, "Shopminer: Mining customer shopping behavior in physical clothing stores with cots rfid devices," in *Proceedings of the 13th ACM Conference on Embedded Networked Sensor Systems*, SenSys '15, (New York, NY, USA), pp. 113–125, ACM, 2015.

[20] S. Pradhan, E. Chai, K. Sundaresan, L. Qiu, M. A. Khojastepour, and S. Rangarajan, "Rio: A pervasive rfid-based touch gesture interface," in *Proceedings of the 23rd Annual International Conference on Mobile Computing and Networking*, MobiCom '17, pp. 261–274, 2017.

[21] C. Occhiuzzi and G. Marrocco, "Constrained-design of passive uhf rfid sensor antennas," *IEEE Transactions on Antennas and Propagation*, vol. 61, pp. 2972–2980, June 2013.

[22] R. Bhattacharyya, C. Floerkemeier, and S. E. Sarma, "Low-cost, ubiquitous rfid-tag-antenna-based sensing," *Proceedings of the IEEE*, vol. 98, pp. 1593–1600, 2010.

[23] M. C. Caccami, S. Manzari, and G. Marrocco, "Phase-oriented sensing by means of loaded uhf rfid tags," *IEEE Transactions on Antennas and Propagation*, vol. 63, pp. 4512–4520, Oct 2015.

[24] J. Wang, O. Abari, and S. Keshav, "Challenge: Rfid hacking for fun and profit," in *Proceedings of the 24th Annual International Conference on Mobile Computing and Networking*, MobiCom '18, (New York, NY, USA), pp. 461–470, ACM, 2018.

[25] C. Occhiuzzi and G. Marrocco, "Precision and accuracy in uhf-rfid power measurements for passive sensing," *IEEE Sensors Journal*, vol. 16, pp. 3091–3098, 2016.

[26] "Impinj speedway uhf rfid reader." https://www.impinj.com/products/readers/.

[27] D. Avrahami and S. E. Hudson, "Forming interactivity: A tool for rapid prototyping of physical interactive products," in *Proceedings of the 4th Conference on Designing Interactive Systems: Processes, Practices, Methods, and Techniques*, 2002.

[28] N. Marquardt, A. S. Taylor, N. Villar, and S. Greenberg, "Rethinking rfid: Awareness and control for interaction with rfid systems," in *Proceedings of the SIGCHI Conference on Human Factors in Computing Systems*, CHI '10, (New York, NY, USA), pp. 2307–2316, ACM, 2010.

[29] D. Yeager, A. Sample, and J. Smith, *Wisp: A passively powered uhf rfid tag with sensing and computation*. 01 2008.

[30] P. Zhang, P. Hu, V. Pasikanti, and D. Ganesan, "Ekhonet: High speed ultra low-power backscatter for next generation sensors," in *Proceedings of the 20th Annual International Conference on Mobile Computing and Networking*, MobiCom '14, (New York, NY, USA), pp. 557–568, ACM, 2014.

[31] Y. Ma, N. Selby, and F. Adib, "Minding the billions: Ultra-wideband localization for deployed rfid tags," in *Proceedings of the 23rd Annual International Conference on Mobile Computing and Networking*, MobiCom '17, pp. 248–260, ACM, 2017.

[32] T. Wei and X. Zhang, "Gyro in the air: Tracking 3d orientation of batteryless internet-of-things," in *Proceedings of the 22Nd Annual International Conference on Mobile Computing and Networking*, MobiCom '16, (New York, NY, USA), pp. 55–68, ACM, 2016.

[33] C. Gao, Y. Li, and X. Zhang, "Livetag: Sensing human-object interaction through passive chipless wifi tags," in *15th USENIX Symposium on Networked Systems Design and Implementation (NSDI 18)*, (Renton, WA), pp. 533–546, USENIX Association, 2018.

[34] "Eval01-fenix-rm tag datasheet." http://www.farsens.com/wp-content/uploads/2018/09/DS-EVAL01-FENIX-RM-V04.pdf.

[35] "Farsens eval01-fenix-rm uhf tag." http://www.farsens.com/en/products/eval01-fenix-rm/.

[36] J. Yin, J. Yi, M. K. Law, Y. Ling, M. C. Lee, K. P. Ng, B. Gao, H. C. Luong, A. Bermak, M. Chan, W. Ki, C. Tsui, and M. Yuen, "A system-on-chip epc gen-2 passive uhf rfid tag with embedded temperature sensor," *IEEE Journal of Solid-State Circuits*, vol. 45, no. 11, pp. 2404–2420, 2010.

[37] "Uhf 915 mhz temperature sensing rfid tags." https://www.rfidinc.com/uhf-915-mhz-temperature-sensing-rfid-tags.

[38] "Rfm3200 wireless flexible temperature sensor." https://axzon.com/rfm3200-wireless-flexible-temperature-sensor/.

[39] A. A. Babar, S. Manzari, L. Sydanheimo, A. Z. Elsherbeni, and L. Ukkonen, "Passive uhf rfid tag for heat sensing applications," *IEEE Transactions on Antennas and Propagation*, vol. 60, pp. 4056–4064, Sep. 2012.

[40] S. Amendola, G. Bovesecchi, A. Palombi, P. Coppa, and G. Marrocco, "Design, calibration and experimentation of an epidermal rfid sensor for remote temperature monitoring," *IEEE Sensors Journal*, vol. 16, pp. 7250–7257, Oct 2016.

[41] G. Marrocco and F. Amato, "Self-sensing passive rfid: From theory to tag design and experimentation," in *2009 European Microwave Conference (EuMC)*, pp. 001–004, Sept 2009.

[42] G. Marrocco, "Pervasive electromagnetics: sensing paradigms by passive rfid technology," *IEEE Wireless Communications*, vol. 17, pp. 10–17, December 2010.

[43] S. Capdevila, L. Jofre, J. Romeu, and J. C. Bolomey, "Passive rfid based sensing," in *2011 IEEE International Conference on RFID-Technologies and Applications*, pp. 507–512, Sep. 2011.

[44] S. Milici, S. Amendola, A. Bianco, and G. Marrocco, "Epidermal rfid passive sensor for body temperature measurements," in *2014 IEEE RFID Technology and Applications Conference (RFID-TA)*, pp. 140–144, Sept 2014.

[45] R. Bhattacharyya, C. Floerkemeier, and S. Sarma, "Rfid tag antenna based sensing: Does your beverage glass need a refill?," in *2010 IEEE International Conference on RFID (IEEE RFID 2010)*, pp. 126–133, April 2010.

[46] S. Manzari, A. Catini, G. Pomarico, C. D. Natale, and G. Marrocco, "Development of an uhf rfid chemical sensor array for battery-less ambient sensing," *IEEE Sensors Journal*, vol. 14, pp. 3616–3623, Oct 2014.

[47] S. Manzari, C. Occhiuzzi, S. Nawale, A. Catini, C. D. Natale, and G. Marrocco, "Humidity sensing by polymer-loaded uhf rfid antennas," *IEEE Sensors Journal*, vol. 12, pp. 2851–2858, Sept 2012.

[48] C. Occhiuzzi, A. Rida, G. Marrocco, and M. Tentzeris, "Rfid passive gas sensor integrating carbon nanotubes," *IEEE Transactions on Microwave Theory and Techniques*, vol. 59, pp. 2674–2684, Oct 2011.

[49] S. Caizzone, E. Digiampaolo, and G. Marrocco, "Investigation of suitable parameters for setup-independent rfid sensing," in *2015 International EURASIP Workshop on RFID Technology (EURFID)*, pp. 98–102, Oct 2015.

[50] G. Marrocco, "Rfid grids: Part i—electromagnetic theory," *IEEE Transactions on Antennas and Propagation*, vol. 59, pp. 1019–1026, March 2011.

[51] U. Ha, J. Leng, A. Khaddaj, and F. Adib, "Food and liquid sensing in practical environments using rfids," in *17th USENIX Symposium on Networked Systems Design and Implementation (NSDI 20)*, (Santa Clara, CA), pp. 1083–1100, USENIX Association, 2020.

[52] S. N. R. Kantareddy, R. Bhattacharyya, and S. Sarma, "Uhf rfid tag ic power mode switching for wireless sensing of resistive and electrochemical transduction modalities," in *2018 IEEE International Conference on RFID (RFID)*, pp. 1–8, 2018.

[53] "Epc/rfid llrp standards." http://www.gs1.org/epcrfid/epc-rfid-llrp/1-1-0.

[54] "Octane sdk for impinj." https://support.impinj.com/hc/en-us/articles/202755268-Octane-SDK.

[55] P. V. Nikitin, K. V. S. Rao, S. Member, and S. Lazar, "An overview of near field uhf rfid," 2007.

[56] U. Karthaus and M. Fischer, "Fully integrated passive uhf rfid transponder ic with 16.7-/spl mu/w minimum rf input power," *IEEE Journal of Solid-State Circuits*, vol. 38, pp. 1602–1608, Oct 2003.

[57] "Speedway revolution reader application note low level." http://bit.ly/2geiFVA.
[58] S. Manzari, C. Occhiuzzi, S. Nawale, A. Catini, C. Di Natale, and G. Marrocco, "Humidity sensing by polymer-loaded uhf rfid antennas," *IEEE Sensors Journal*, vol. 12, pp. 2851–2858, Sep. 2012.
[59] R. Bhattacharyya, C. Floerkemeier, and S. Sarma, "Low-cost, ubiquitous rfid-tag-antenna-based sensing," *Proceedings of the IEEE*, vol. 98, pp. 1593–1600, Sep. 2010.
[60] C. H. Loo, K. ElMahgoub, F. Yang, A. Elsherbeni, D. Kajfez, A. Kishk, T. Elsherbeni, L. Ukkonen, L. Sydänheimo, M. Kivikoski, and o. , "Chip impedance matching for uhf rfid tag antenna design," *Progress In Electromagnetics Research*, vol. 81, pp. 359–370, 01 2008.
[61] P. V. Nikitin, K. V. S. Rao, and R. D. Martinez, "Differential rcs of rfid tag," *Electronics Letters*, vol. 43, pp. 431–432, April 2007.
[62] K. V. S. Rao, S. Member, P. V. Nikitin, and E. F. Lam, "Antenna design for uhf rfid tags: A review and a practical application," *IEEE Trans. Antennas Propag*, pp. 3870–3876, 2005.
[63] D. M. Dobkin, *The RF in RFID, Second Edition: UHF RFID in Practice.* Newton, MA, USA: Newnes, 2nd ed., 2012.
[64] M. Bolic, D. Simplot-Ryl, and I. Stojmenovic, *RFID Systems: Research Trends and Challenges.* Wiley Publishing, 1st ed., 2010.
[65] G. Marrocco, "The art of uhf rfid antenna design: impedance-matching and size-reduction techniques," *IEEE Antennas and Propagation Magazine*, vol. 50, pp. 66–79, Feb 2008.
[66] C. Occhiuzzi and G. Marrocco, "Constrained-design of passive uhf rfid sensor antennas," *IEEE Transactions on Antennas and Propagation*, vol. 61, pp. 2972–2980, June 2013.
[67] K. Steinberg, M. Scheffler, and M. Dressel, "Microwave inductance of thin metal strips," 2010.
[68] C. A. Balanis, *Antenna Theory: Analysis and Design.* New York, NY, USA: Wiley-Interscience, 2005.
[69] G. E. Ponchak, J. L. Jordan, and M. C. Scardelletti, "Temperature dependence of thin film spiral inductors on alumina over a temperature range of 25 to 475° c," in *2010 Proceedings 60th Electronic Components and Technology Conference (ECTC)*, pp. 713–719, June 2010.
[70] "Ansys hfss: 3d electromagnetic field simulator for rf and wireless design." https://www.ansys.com/products/electronics/ansys-hfss.
[71] "High frequency lcr meter." https://hiokiusa.com/product/impedance-analyzer-im3570/.
[72] A. P. Sohrab, Y. Huang, M. Hussein, M. Kod, and P. Carter, "A uhf rfid tag with improved performance on liquid bottles," *IEEE Antennas and Wireless Propagation Letters*, vol. 15, pp. 1673–1676, 2016.
[73] N. Tran, B. Lee, and J. Lee, "Development of long-range uhf-band rfid tag chip using schottky diodes in standard cmos technology," in *2007 IEEE Radio Frequency Integrated Circuits (RFIC) Symposium*, pp. 281–284, 2007.
[74] "Array Solutions VNA-UHF - Two Port Vector Network Analyzer, 5 kHz to 1200 MHz." https://www.arraysolutions.com/vna-uhf.
[75] M. C. Caccami and G. Marrocco, "Electromagnetic modeling of self-tuning rfid sensor antennas in linear and nonlinear regimes," *IEEE Transactions on Antennas and Propagation*, vol. 66, pp. 2779–2787, June 2018.
[76] H. Rahul, F. Edalat, D. Katabi, and C. Sodini, "Frequency-aware rate adaptation and mac protocols," in *Proc. of MobiCom*, 2009.
[77] "Fisher scientific isotemp 637g oven." https://www.marshallscientific.com/Fisher-Scientific-Isotemp-637G-Oven-p/Fi-637G.htm.
[78] "Arduino uno r3." https://www.amazon.com/Arduino-A000066-ARDUINO-UNO-R3/dp/B008GRTSV6/.
[79] "Bme280 pressure temperature sensor module." https://www.amazon.com/Diymall-Pressure-Temperature-Sensor-Arduino/dp/B0118XCKTG/.
[80] "UHF RFID Tags." https://www.atlasrfidstore.com/rfid-tags/.
[81] "Usrp n210." https://www.ettus.com/all-products/un210-kit/.
[82] "Sbx 400-4400 mhz rx/tx (40 mhz)." https://www.ettus.com/all-products/sbx/.
[83] "Rfmax indoor rfid antenna." https://www.atlasrfidstore.com/rfmax-s9028pcr-s8658pcr-rhcp-indoor-rfid-antenna-fcc-etsi/.
[84] "Gen2 uhf rfid reader with usrp and gnu radio." https://github.com/nkargas/Gen2-UHF-RFID-Reader/.
[85] "Copper foil 110 annealed." https://bit.ly/2Fnet5b.
[86] D. D. Deavours, K. Demarest, A. Syed, D. D. Deavours, K. Demarest, and A. Syed, "Effects of antenna material on the performance of uhf rfid tags," in *2007 IEEE International Conference on RFID*, pp. 57–62, March 2007.
[87] "Nxp semiconductors sl3s1002ftb1,115." https://bit.ly/2W9Sswc.
[88] "Fr4 copper-clad board." https://www.amazon.com/MG-Chemicals-Copper-Board-Single/dp/B008OAFKUS/.
[89] "Raspberry pi 3 model b." https://www.raspberrypi.org/products/raspberry-pi-3-model-b/.
[90] J. Wang, J. Zhang, R. Saha, H. Jin, and S. Kumar, "Pushing the range limits of commercial passive rfids," in *16th USENIX Symposium on Networked Systems Design and Implementation (NSDI 19)*, (Boston, MA), pp. 301–316, USENIX Association, Feb. 2019.